ELSEVIER

Journal of Organometallic Chemistry 557 (1998) 13–28

Journal of Organometallic Chemistry

Structure and reactivity of the zero-valent ruthenium complex Ru(1,2-bis(diphenylphosphino)ethane)$(CO)_3$ and the dicationic ruthenium dimer $[Ru_2(1,2\text{-bis(diphenylphosphino)ethane})_2(CO)_6]^{2+}$

Steven J. Skoog, Amy L. Jorgenson, John P. Campbell, Michelle L. Douskey, Eric Munson, Wayne L. Gladfelter *

Department of Chemistry, The University of Minnesota, 207 Pleasant St. SE, Minneapolis, MN 55455, USA

Received 25 May 1997

Abstract

The structure of Ru(dppe)$(CO)_3$ was characterized by single crystal X-ray diffraction [monoclinic crystal system, space group $P2_1/n$, $a = 12.2353(2)$ Å, $b = 16.0803(3)$ Å, $c = 14.2451(3)$ Å, $\beta = 111.109(1)°$, $V = 2614.62(9)$ Å^3, $Z = 4$] and found to be intermediate between trigonal bipyramidal and square pyramidal. One electron oxidation of Ru(dppe)$(CO)_3$ using $[(\eta^5\text{-}C_5H_5)_2Fe][PF_6]$ produced $[Ru_2(dppe)_2(CO)_6][PF_6]_2$. The dicationic complex was fully characterized by solution spectroscopic methods and by single crystal X-ray diffraction [trigonal crystal system, space group $P3_121$, $a = 20.566(2)$ Å, $c = 13.871(2)$ Å, $V = 5080.7(8)$ Å^3, $Z = 3$] and found to have a dimeric structure with two octahedral units sharing a common apex via a Ru(I)–Ru(I) single bond. One octahedral unit is rotated approximately 45° relative to the other, and the chelating phosphine ligand occupies sites cis and trans to the Ru(I)–Ru(I) bond. All of the carbonyl ligands were found to be terminal. The dimer was fluxional in solution and line-shape analysis of the $^{31}P\{^1H\}$ and $^{13}C\{^1H\}$ variable-temperature NMR spectra was used to investigate the exchange mechanism and evaluate the rate constants. The mechanism involved an intramolecular, two-site exchange involving pairwise bridging carbonyls and had activation parameters of 11.8 ± 0.15 kcal mol^{-1} and -6.7 ± 0.6 eu for $\Delta H^{\ddagger}$ and $\Delta S^{\ddagger}$ respectively. The dimer exhibited similar thermal and photochemical reactivity patterns; disproportionation occurred in CH_3CN and halogen atom abstraction occurred in halogenated solvents.

Keywords: Ruthenium; Carbonyl; Crystal structure; Dynamic NMR; Photochemistry; Metal-centered radicals

1. Introduction

During the course of our study of the activation of nitroarenes by Ru(dppe)$(CO)_3$ (**1**), where dppe is 1,2-bis(diphenylphosphino)ethane, we became interested in the properties of the radical cation formed by oxidation of **1** due to its importance as a potential intermediate in Eq. (1) [1–4]. Radical processes play a large role in the reaction mechanisms of organometallic

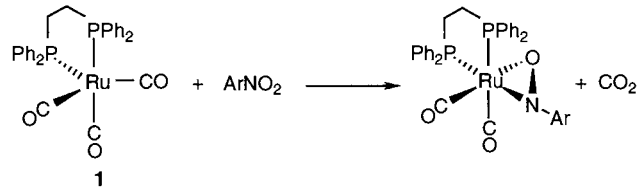

1

species and are important in both stoichiometeric and catalytic reactions [5]. Iron-centered radicals formed from bis(phosphine) carbonyl complexes generated electrochemically [6] or chemically [7] were found to undergo a variety of radical coupling [8], substitution [9], and disproportionation reactions [10,11], and have been

* Corresponding author. Tel.: +1 612 6244391; fax: +1 612 6267541; e-mail: gladfelt@chemsun.chem.umn.edu

0022-328X/98/$19.00
PII S0022-328X(97)00731-6

extensively studied [12,13]. Bis(phosphine) substituted ruthenium(I) radical carbonyl complexes exhibit similar reactivity to that of their iron analogs [2,14].

2. Experimental

2.1. General

Standard Schlenk techniques were used in handling all organometallic compounds [15]. A nitrogen-filled Vacuum Atmospheres dry box equipped with a Dri-Train Model 40-1 inert gas purifier or a MBraun 150-M dry box were used for manipulations requiring inert atmosphere conditions. The compounds 1,2-bis(-diphenylphosphino)ethane and $Ru_3(CO)_{12}$ were purchased from Strem and the former was purified by recrystallization from hexane/toluene. Ferrocenium hexafluorophosphate was prepared according to literature procedures [16]. Solvents were distilled prior to use under pre-purified nitrogen; toluene and hexane were distilled from purple sodium benzophenone ketyl where small amounts of triglyme were used to solubilize the anion in hexane. Methylene chloride, 1,2-dichloroethane and deuterated methylene chloride were distilled from calcium hydride and stored under a nitrogen atmosphere over 4 Å molecular sieves. Acetonitrile and deuterated acetonitrile were either distilled from CaH_2 under a nitrogen atmosphere and either used immediately or stored under nitrogen over 4 Å molecular sieves. Deuterated dimethyl ether was prepared using literature procedures [17]. Carbon monoxide (CP grade) and ^{13}CO (Isotech 99.2 atom % ^{13}C) were used without further purification. All infrared spectral measurements were carried out on a Mattson Polaris FTIR spectrometer. The ^1H-, $^{13}C\{^1H\}$-, and $^{31}P\{^1H\}$-NMR spectral studies were performed using a Varian VXR-300 spectrometer operating at 300, 75.4 and 121.4 MHz respectively. All $^{31}P\{^1H\}$-NMR spectra were externally referenced to 85% D_3PO_4 (0.0 ppm) or (wherever possible) internally referenced to $[PF_6]^-$ (-141 ppm). Proton and $^{13}C\{^1H\}$-NMR spectra were referenced to resonances corresponding to residual protons or carbon atoms of the solvent. Electron paramagnetic resonance (EPR) spectral measurements were made on a ESP 300 spectrometer using a quartz sample tube. Ultraviolet spectra were obtained on a HP 8452A diode array spectrometer at various concentrations and the molar absorptivity was obtained from a Beer's law plot. Photolysis experiments were carried out using a 175 W medium pressure Hg vapor lamp. High pressure NMR experiments were carried out in a sapphire NMR tube [18]. Thermal and photochemical reactivity experiments were carried out in glass or quartz NMR tubes, respectively, capped with a septum under a nitrogen atmosphere, and sealed with Teflon tape and Parafilm. The quartz NMR tubes were cooled during photolysis with a water-jacketed quartz Schlenk tube in an ethanol bath.

2.2. Synthesis of $Ru(dppe)(CO)_3$ (1)

A slightly modified version of the original procedure was used [19]. Ruthenium carbonyl (1.99 g, 3.13 mmol) and dppe (3.74 g, 9.40 mmol) were placed in a 250 ml Parr autoclave, toluene (20 ml) was added, purged three times with CO, charged to 68 atm, and finally heated at 125°C for 18 h. The resulting yellow solution was filtered through a plug of glass wool and transferred to a 100 ml flask capped with a septum, purged with N_2 and layered with 30 ml of hexane. Large yellow crystals were grown at room temperature and collected on a glass frit. The crystals were washed with hexane and dried yielding 4.86 g of $Ru(dppe)(CO)_3$ (89% yield). Samples were stored in a glove box. mp: 120° (dec). IR (cm^{-1}, CH_2Cl_2): ν_{CO} 1910 (s), 1931 (s), 2001 (s). ^1H-NMR (ppm, CH_2Cl_2, RT) δ 2.41 (d, $J_{HP} = 20.4$ Hz, CH_2); 7.42 (m, ArH); 7.63 (m, ArH). $^{31}P\{^1H\}$-NMR (ppm, CH_2Cl_2, RT) δ 74.6 (s, dppe, $T_1 = 2.23 \pm 0.03$ s at 23°C). $^{13}C\{^1H\}$-NMR (ppm, CD_2Cl_2, RT) δ 30.99 (t, $J_{CP} = 24.7$ Hz, CH_2); 128.97 (t, $J_{CP} = 4.86$ Hz, *m*, C_6H_5); 130.52 (s, *p*, C_6H_5); 132.62 (t, $J_{CP} = 6.1$ Hz, *o*, C_6H_5); 137.52 (m, $J_{CP} = 18.8$ Hz, ipso, C_6H_5); 211.84 (t, $J_{CP} = 10.67$ Hz, *C*O).

2.3. Synthesis of $Ru(dppe)(CO)_{3-x}(^{13}CO)_x$

2.3.1. Method A

A 1 ml volumetric flask was loaded with 18.9 mg (0.0324 mmol) of $Ru(dppe)(CO)_3$ and filled to 1 ml with C_6D_6 in the glove box. One-half of this solution was transferred via syringe into a high-pressure sapphire NMR tube. The NMR tube was attached to a stainless steel manifold and evacuated. The head space of the NMR tube was pressurized to 155 psig with ^{13}CO. The tube was heated at 100°C for 2 h. Analysis of the $^{31}P\{^1H\}$-NMR spectrum showed that the ratio of non-labeled to mono-labeled to di-labeled **1** was 3:5:2.

2.3.2. Method B

A thick-walled 15 ml flask with an attached ground glass joint and Kontes valve was loaded with 1.01 g (1.73 mmol) of $Ru(dppe)(CO)_3$ in a glove box. The flask was removed from the box, 4 ml of toluene was added, three freeze-pump-thaw cycles were completed and after cooling to -196°C, one equivalent of ^{13}CO was condensed into the flask using a calibrated gas ballast at a known pressure. After warming to room temperature, the flask was heated to 80°C for 22 h. Analysis by $^{31}P\{^1H\}$-NMR indicated ca. 6:4:1 ratio of non-labeled to mono-labeled to di-labeled **1**. The sample was then transferred to a 50 ml Erlenmeyer flask

and layered with 20 ml of hexanes to give 900 mg of crystalline product (90% yield) that was collected on a glass frit and dried under vacuum.

2.4. Synthesis of $[Ru_2(dppe)_2(CO)_6][PF_6]_2$ (2)

A 50 ml round-bottom Schlenk flask was loaded with 314 mg (0.538 mmol) of **1**, and a solid addition flask was loaded with 158 mg (0.477 mmol) of $[Cp_2Fe][PF_6]$. The flask was removed from the glove box and 9 ml of CH_2Cl_2 was added via syringe and cooled to −78°C. After the solution was cool, the $[Cp_2Fe][PF_6]$ was slowly added over a 45 min period and allowed to stir at −78°C for 2 h after complete addition of the oxidant. The reaction solution was allowed to warm slowly to 0°C, and the CH_2Cl_2 was reduced to ca. 3 ml. The concentrated solution was then cooled again to −78°C and 30 ml of hexanes was added via syringe to the rapidly stirring solution, to precipitate **2** as a yellow solid. The solid material was filtered at −78°C on a glass frit, washed with toluene to remove excess **1** and finally dried under vacuum for several hours to give 330 mg of **2** (84% yield). This same procedure was used with ^{13}CO-labeled **1** as starting material to afford ^{13}CO-labeled **2**. The reaction was also successfully scaled up to 1.0 g of **1** with appropriate increases of oxidant and carried out in 20 ml of CH_2Cl_2. IR (cm^{-1}, CH_2Cl_2) ν_{CO} 2102 (w); 2062 (m); 2039 (vs). UV (CH_2Cl_2); $\lambda = 386$ nm ($\epsilon = 17500\ M^{-1}\ cm^{-1}$). ^1H-NMR (ppm, CH_2Cl_2, RT) δ 2.88 (br, CH_2, 2H); 2.95 (br, CH_2, 2H); 7.39–7.61 (ArH, 20H). $^{31}P\{^1H\}$-NMR (ppm, CH_2Cl_2, RT) δ 56.76 (br, dppe, $T_1 = 1.74 \pm 0.14$ s at 23°C); 46.47 (br, dppe, $T_1 = 1.62 \pm 0.07$ s at 23°C); −141.0 (septet, $J_{PF} = 710.6$ Hz, PF_6^-, $T_1 = 5.48 \pm 0.07$ s at 23°C). $^{13}C\{^1H\}$NMR (see Results). Anal. Calcd. for **2**: C, 47.81; H, 3.32. Found: C, 47.72; H, 3.15.

2.5. Synthesis of $[Ru(dppe)(CO)_2(CH_3CN)_2][PF_6]_2$ (3)

A Schlenk tube was charged with 300 mg (0.206 mmol) of **2** followed by addition of 10 ml of CH_3CN and refluxed for 45 min. Analysis by IR spectroscopy indicated a 1:1 mixture of **1** and **3**. The solvent (CH_3CN) was completely removed by vacuum and 3 ml of CH_2Cl_2 was added to the red oil. 30 ml of toluene was added yielding a red oily precipitate and a yellow supernatant. The mixture was cooled to −78°C and a red/brown precipitate formed. The solid was filtered and washed with toluene until the washings were colorless. The material was recrystallized from CH_2Cl_2/ hexane (1:10) to give 106 mg (56% yield) of **3**. In order to obtain analytically pure material the compound was dissolved in CH_3CN, evaporated to dryness, and finally recrystallized from CH_2Cl_2/pentane (1:10). IR (cm^{-1}, CH_2Cl_2) ν_{CO} 2032 (vs); ν_{CN} 2299 (w), 2323 (w). ^1H-NMR (ppm, CD_2Cl_2, RT) δ 2.58 (s, NCCH_3, 6H); 2.92 (m, −CH_2, 2H); 3.22 (m, −CH_2, 2H); 7.59–7.65 (ArH, 20H). $^{31}P\{^1H\}$-NMR (ppm, CD_2Cl_2, RT) δ 64.75 (s, dppe); −141.0 (septet, $J_{PF} = 710.6$ Hz, PF_6). $^{13}C\{^1H\}$-NMR (ppm, CD_2Cl_2, RT) δ 4.16 (s, NCCH_3); 26.59 (m, CH_2), 130.28 (t, $J_{CP} = 4.9$ Hz, aryl); 130.41 (t, $J_{CP} = 5.4$ Hz, aryl); 131.72 (t, $J_{CP} = 4.6$ Hz, aryl); 131.99 (t, $J_{CP} = 4.9$ Hz, aryl); 132.87 (s, aryl); 133.19 (s, aryl); 195 (t, $J_{CP} = 15.5$ Hz, CO). Anal. Calcd for **3** · CH_3CN: C, 42.16; H, 3.43; N, 4.33. Found: C, 42.95; H, 3.92; N, 4.03.

2.6. Synthesis of $[Ru(dppe)(CO)_3Cl][PF_6]$ (5)

A water-jacketed quartz Schlenk flask was charged with 200 mg (0.137 mmol) of **2** in a glove box followed by addition of 20 ml of 1,2-$C_2H_2Cl_2$ and photolyzed for 16 h at 25°C. The resulting solution was transferred via filter cannula to a round-bottom flask, and the solvent was completely removed under vacuum. 3 ml of CH_2Cl_2 were added to dissolve the residue, followed by 30 ml of hexanes, and a light brown oil formed on the bottom of the flask. The flask was cooled to −78°C, and the walls were scraped to loosen the solidified oil. The precipitate was filtered at −78°C, yielding 146 mg of crude microcrystalline tan product (70% yield). Subsequent repeated recrystallization from CH_2Cl_2/pentane (1:10) provided the analytically pure material. IR (cm^{-1}, CH_2Cl_2) ν_{CO} 2135 (vs), 2097.5 (s), 2053 (s). ^1H-NMR (ppm, CD_2Cl_2, RT) δ 3.13 (m, −CH_2, 2H); 3.45 (m, −CH_2, 2H); 7.52–7.59 (m, ArH, 20H). $^{31}P\{^1H\}$-NMR (ppm, CD_2Cl_2, RT) δ 54.51 (s, dppe); −141.0 (septet, $J_{PF} = 711$ Hz, PF_6). $^{13}C\{^1H\}$-NMR (ppm, CD_2Cl_2, RT) δ 25.55 (m, CH_2); 129.72 (t, $J_{CP} = 5.5$ Hz, aryl); 130.79 (t, $J_{CP} = 5.1$ Hz, aryl); 132.34 (t, $J_{CP} = 4.9$ Hz, aryl); 132.81 (t, $J_{CP} = 4.5$ Hz, aryl); 132.98 (s, aryl); 133.64 (s, aryl); 184.64 (dd, $J_{CP1} = 95.16$ Hz; $J_{CP2} = 13.42$ CO); 187.02 (t, $J_{CP} = 11.76$ Hz, CO). Anal. Calcd for **4**: C, 45.59; H, 3.15; Cl, 4.64. Found: C, 45.73; H, 3.25; Cl, 4.46.

2.7. Variable-temperature NMR spectroscopy

For variable-temperature NMR experiments the thermocouple was calibrated against a neat ethylene glycol standard at elevated temperature, neat methanol near room temperature [20]. The low-temperature (< −20°C) calibration utilized a mixture of CH_3OH with 6% HCl (by volume) to −40, and CH_3OH/HCl/CH_2Cl_2 in a 10:1:20 ratio down to −110. Both of these solutions were calibrated in a higher temperature range. Measurements of T_1 were made using the inversion recovery method (180–τ–90), and the data processed using Varian Software.

Unless otherwise noted samples for the dynamic NMR experiments were loaded in a glove box into NMR tubes with ground glass joints and attached to a

Schlenk line. Solvent was vacuum distilled into the tube, which was cooled to −78°C. The mixture was cooled to −198°C and sealed under vacuum. To prepare the NMR sample of $Ru(dppe)(CO)_{3-x}(^{13}CO)_x$ in $(CD_3)_2O$, 0.1 ml of the solution of labeled **1**, prepared as described in Method A was dried in vacuo for 30 min, and 0.2 ml of $(CD_3)_2O$ was vacuum transferred to give a 16 mM solution.

Variable-temperature NMR experiments with **2** utilized 37 mM solutions. Different solvents were used in different temperature regimes: CD_2Cl_2 was used as the solvent in a sealable NMR tube below 30°C; 1,2-$C_2H_4Cl_2$/CD_2Cl_2 (3:1 by volume) was used as the solvent in a sealable NMR tube up to 60°C; and 1,2-$C_2H_4Cl_2$/CD_2Cl_2 (3:1) was used as the solvent in a high-pressure sapphire NMR tube up to 90°C. Experiments run at elevated temperatures(> 40°C) were recorded as rapidly as possible to minimize decomposition of **2**.

Spin simulations were carried out using the DSYMPC program [21], available from Düsseldorf University, spectral deconvolution and adjusted weighting of broadened peaks were accomplished using the Varian software. Complete line-shape analysis for the variable-temperature $^{31}P\{^1H\}$- and $^{13}C\{^1H\}$-NMR spectra of **2** was carried out using DNMR5 (QCMP 059) available from the QCPE at Indiana University.

2.8. Solid-state NMR spectroscopy

All solid-state NMR experiments were performed on a Chemagnetics CMX Infinity 300 MHz spectrometer operating at 75.4 MHz for ^{13}C and 121.4 MHz for ^{31}P using cross-polarization (CP) [22], magic-angle spinning (MAS), and high-power ^1H decoupling. A standard Chemagnetics pencil probe equipped with a variable-temperature accessory was used to spin a zirconia rotor at 4–5 kHz. Single-contact cross polarization with high-power proton decoupling (90° pulse width = 4 μs, pulse delay = 180.0 s, 128 transients) was used to acquire the ^{13}C spectrum used in this study. The methyl resonance of hexamethylbenzene was used as an external reference and set to 17.35 ppm. A single-contact cross polarization sequence was also used to acquire the ^{31}P spectrum (90° pulse width = 4 μs, pulse delay = 10.0 s, 48 transients.) A fresh sample of triphenylphosphine was used as a reference and set at −11.9 ppm.

2.9. X-ray structural analysis of *1* and *2*

Single crystals were grown from hexane/toluene for **1** and hexane/CH_2Cl_2 for **2**. Table 1 includes a summary of the details of the crystallographic data. A suitable crystal was selected and mounted on the tip of a glass fiber with STP oil. It was transferred to the goniometer of a Siemens SMART CCD System and cooled to −100° with a Siemens LT-2 low-temperature device. Crystal quality and centering was confirmed by taking a 60s rotation frame. A search was performed by taking a series of frames in three orthogonally related regions of reciprocal space. Each region investigated was comprised of 20 ten second frames, 0.3° apart in omega.

Table 1
Summary of crystallographic data for **1** and **2**

Crystal Parameters		
Compound	**1**	**2**
Crystal system	monoclinic	trigonal
Space group	$P2_1/n$	$P3_121$
Formula	$C_{29}H_{24}O_3P_2Ru$	$C_{58}H_{48}F_{12}O_6P_6Ru_2$
Formula weight (g mol^{-1})	583.49	1456.92
Unit cell dimensions		
a (Å)	12.2353(2)	20.566(2)
b (Å)	16.0803(3)	20.566(2)
c (Å)	14.2451(3)	13.871(2)
α (°)	90	90
β (°)	111.109(1)	90
γ (°)	90	120
V (Å^3)	2614.62(9)	5080.7(8)
Z	4	3
ρ(calcd.) (g cm^{-3})	1.482	1.761
Temperature (K)	173(2)	174(2)
Abs coeff (mm^{-1})	0.751	0.664
Cryst dimens (mm)	0.5 × 0.25 × 0.12	0.468 × 0.26 × 0.156
Trans. factors, max to min %	0.623–0.554	0.752–0.642
Measurement of intensity data		
Diffractometer	Siemens SMART Platform CCD	
Radiation	Mo-K$_\alpha$ (0.71073 Å)	
Monochromator	graphite	
Abs corr applied	Semiempirical	
No. of reflns measd	11008	25234
No. of unique reflns	4240	5414
No. of reflns used	4240	5412
Solution and refinement		
Programs used	SHELXTL-V5.0	
Method of structure solution	Direct methods	
Adjusted weighting scheme	$w=[\sigma^2(F_o^2)+(AP)^2+(BP)]^{-1}$, where $P=(F_o^2+2F_c^2))/3$	
Constants for weighting	$A=0.0397$, $B=2.9317$	$A=0.0248$, $B=4.19$
Final R^a indices [$I>2\sigma(I)$]	$R_1=0.0327$, $wR^2=0.0808$	$R_1=0.0281$, $wR^2=0.0611$
R^a indices (all data)	$R_1=0.0362$, $wR_2=0.0836$	$R_1=0.0313$, $wR_2=0.0655$
Goodness-of-fit on F^2	1.067	1.053

[a] $R_1=\dfrac{\Sigma\,\|F_o\|-|F_c\|}{\Sigma|F_o|}$ $\qquad wR^2=\left[\dfrac{\Sigma[w(F_o^2-F_c^2)^2]}{\Sigma[w(F_o^2)^2]}\right]^{1/2}$

These were harvested to yield a total of about 100 reflections with intensities greater than 10 s. An initial unit cell was obtained, and checked for centering and higher symmetry. None was found. The initial cell constants were refined, and an initial orientation matrix was found. Data were collected by examining a randomly oriented region of reciprocal space in three segments; the frames collected in a given segment were 0.3° apart in omega. The highest resolution data collected was 0.87 Å. The total shutter open time for each double-correlated frame was 60 s; two 30 s frames were collected, and the data summed, doubling the dynamic range of the detector. The default gain on the detector signal was 4×, which was automatically dropped to 1× when the detector range was exceeded. Final cell constants were determined during integration of the data using 8192 intense, well-centered reflections.

The structures were solved and refined using the SHELXTL-plus 5.0 series of programs [23,24]. The space group for **1** was determined to be $P2_1/n$ (# 14) and for **2** to be $P3_121$ (# 152) based on systematic extinctions and intensity statistics. The space group of **2** is chiral; its enantiomer is $P3_221$. The low absolute structure factor (Flack parameter) of 0.01(3) confirms the correct choice of enantiomers. The structures were solved using the direct methods program XS. Hydrogen atoms were placed in calculated positions and refined with a riding model with B values 20% larger than those on the attached carbon atoms. Anisotropic refinement of **1** was then performed and converged to a final $R_1 = 0.0358$ (4σ, based on F^2). For **2**, the hexafluorophosphate ion is rotationally disordered over two positions in a 70/30% ratio. Each fluorine was refined anisotropically with the appropriate occupancy. The ion as a whole was refined with bond length and rigid body constraints. The unit cell contains large open channels running parallel to the *c*-axis that were filled with completely disordered solvent. The contribution of the solvent to the scattering power was determined using the program PLATON; it was found to be equal to 404 electrons. The total volume occupied by the disordered solvent was 959 Å^3. The structure factors were corrected for this solvent using the SQUEEZE option of PLATON [25], reducing *R* from 0.035 to 0.028. The density calculated from the SHELEX software package used a entire volume of the unit cell including the disordered solvent. The reported density was corrected for the extra space occupied by the disordered solvent (see Table 1).

Full anisotropic refinement of all non hydrogen atoms was performed using full-matrix least squares on F^2 using the program XL. A semiempirical psi-scan absorption correction was applied to the data prior to solution and refinement. The final difference map was essentially flat, with maximum and minimum peaks corresponding to 0.71 and −0.33 e Å^{-3}. Scattering factors and anomalous scattering terms were taken the usual sources [26], and the effects of anomalous dispersion were included for the non hydrogen atoms. For **1** selected bond angles and bond distances are listed in Table 2, final atomic coordinates and equivalent isotropic thermal parameters, along with their estimated standard deviations are listed in Table 3. For **2** selected bond angles and bond distances are listed in Table 4, final atomic coordinates and equivalent isotropic thermal parameters, along with their estimated standard deviations are listed in Table 5. The molecular structure of **1** is provided in Fig. 1 and the molecular structure of **2** in Fig. 2.

Table 2
Selected bond distances (Å) and angles (°) for $Ru(P(C_6H_{11})_3)2(CO)_3$

Metal-ligand distances			
Ru(1)–C(1)	1.904 (3)	Ru(1)–C(2)	1.901 (4)
Ru(1)–C(3)	1.935 (3)	Ru(1)–P(1)	2.3612 (7)
Ru(1)–P(2)	2.3641 (8)		
Intraligand distances			
C(1)–O(1)	1.149 (4)	C(2)–O(2)	1.162 (4)
C(3)–O(3)	1.147 (4)	P(1)–C(11)	1.846 (3)
P(1)–C(21)	1.845 (3)	P(1)–C(31)	1.828 (3)
P(2)–C(12)	1.840 (3)	P(2)–C(41)	1.833 (3)
P(2)–C(51)	1.827 (3)		
Ligand-metal-ligand			
C(2)–Ru(1)–C(1)	89.34 (13)	C(2)–Ru(1)–C(3)	115.23 (14)
C(1)–Ru(1)–C(3)	100.00 (12)	C(2)–Ru(1)–P(1)	91.35 (10)
C(1)–Ru(1)–P(1)	163.55 (9)	C(3)–Ru(1)–P(1)	94.57 (9)
C(2)–Ru(1)–P(2)	143.49 (11)	C(1)–Ru(1)–P(2)	87.71 (9)
C(3)–Ru(1)–P(2)	101.10 (9)	P(1)–Ru(1)–P(2)	81.89(3)
Metal carbonyls			
Ru(1)–C(1)–O(1)	177.3 (3)	Ru(1)–C(2)–O(2)	178.2 (3)
Ru(1)–C(3)–O(3)	175.3 (3)		

3. Results

3.1. Structure of Ru(dppe)(CO)$_3$ (1)

Yellow crystals of **1** were grown from a toluene solution by layering with hexane at room temperature and were characterized by single crystal X-ray diffraction. The structure was intermediate between trigonal bipyramidal with apical phosphorus and CO ligands and square pyramidal with an apical carbonyl ligand. The P(1)–Ru–P(2) bond angle of 81.98(3)° was comparable to related ruthenium complexes [3,27], and the remaining bond angles were similar to those determined for the iron analog, Fe(dppe)(CO)$_3$ [28]. The Ru–C and Ru–P bond distances in **1** were ca. 6–7% longer than those observed in Fe(dppe)(CO)$_3$. The five-membered ring of the chelating phosphine was puckered with a dihedral P(1)–C(11)–C(12)–P(2) angle of 50.3°, which falls well within the mean range for torsion angles of

45–55° for various transition metal dppe compounds [28].

In solution the $^{31}P\{^{1}H\}$-NMR spectrum contained a sharp singlet for the two phosphorus nuclei owing to the fluxional behavior of the complex at room temperature. The ^{1}H-NMR spectrum exhibited a doublet for the equivalent methylene units of the dppe bridge due to splitting by phosphorus. This resonance was shifted slightly downfield by 0.3 ppm from the free dppe ligand. The $^{13}C\{^{1}H\}$-NMR spectrum exhibited triplets for the methylene and phenyl carbon atoms. These triplets were thought to be due to virtual coupling to both phosphorus atoms and were observed in other compounds containing the dppe ligand [29]. During the ^{13}CO enrichment of **1** via Method A the observed rate for the isotopic substitution of the carbonyl ligand was 1.2×10^{-2} s^{-1} measured from the intensity of the Ru–CO resonance during the first half-life of the reaction and followed an apparent zero-order dependence on the concentration of **1**.

Table 3
Atomic coordinates ($\times 10^4$) and equivalent isotropic displacement parameters ($Å^2 \times 10^3$) for **1**

Atom	x	y	z	U_{eq}	SOF
Ru(1)	12181 (1)	−1227 (1)	10216 (1)	27 (1)	1
C(1)	11542 (3)	−135 (2)	10091 (2)	34 (1)	1
O(1)	11196 (2)	534 (1)	10046 (2)	47 (1)	1
C(2)	12559 (3)	−1033 (2)	9052 (3)	42 (1)	1
O(2)	12759 (3)	−918 (2)	8325 (2)	61 (1)	1
C(3)	10780 (3)	−1878 (2)	9995 (2)	33 (1)	1
O(3)	9906 (2)	−2220 (1)	9822 (2)	46 (1)	1
P(1)	13458 (1)	−2381 (1)	10672 (1)	27 (1)	1
P(2)	12861 (1)	−1044 (1)	11980 (1)	28 (1)	1
C(11)	13652 (3)	−2664 (2)	11978 (2)	32 (1)	1
C(12)	13931 (3)	−1863 (2)	12594 (2)	34 (1)	1
C(21)	14989 (3)	−2227 (2)	10768 (2)	31 (1)	1
C(22)	15344 (3)	−1473 (2)	10492 (2)	35 (1)	1
C(23)	16503 (3)	−1344 (2)	10588 (3)	40 (1)	1
C(24)	17329 (3)	−1963 (2)	10973 (3)	46 (1)	1
C(25)	16995 (3)	−2712 (2)	11266 (3)	49 (1)	1
C(26)	15834 (3)	−2847 (2)	11154 (3)	41 (1)	1
C(31)	13015 (2)	−3340 (2)	9945 (2)	30 (1)	1
C(32)	12313 (3)	−3292 (2)	8931 (2)	35 (1)	1
C(33)	11982 (3)	−4007 (2)	8349 (2)	41 (1)	1
C(34)	12344 (3)	−4779 (2)	8776 (3)	43 (1)	1
C(35)	13027 (3)	−4837 (2)	9785 (3)	47 (1)	1
C(36)	13362 (3)	−4125 (2)	10368 (2)	41 (1)	1
C(41)	13638 (2)	−91 (2)	12556 (2)	32 (1)	1
C(42)	14171 (3)	391 (2)	12038 (2)	37 (1)	1
C(43)	14794 (3)	1102 (2)	12460 (3)	45 (1)	1
C(44)	14875 (3)	1343 (2)	13412 (3)	48 (1)	1
C(45)	14353 (3)	871 (2)	13944 (3)	49 (1)	1
C(46)	13747 (3)	148 (2)	13526 (2)	42 (1)	1
C(51)	11731 (3)	−1126 (2)	12534 (2)	33 (1)	1
C(52)	10853 (3)	−521 (2)	12285 (2)	42 (1)	1
C(53)	9945 (3)	−571 (3)	12653 (3)	52 (1)	1
C(54)	9916 (3)	−1214 (2)	13287 (3)	53 (1)	1
C(55)	10768 (3)	−1814 (2)	13540 (3)	52 (1)	1
C(56)	11683 (3)	−1771 (2)	13170 (3)	44 (1)	1

U_{eq} is defined as one third of the trace of the orthogonalized U_{ij} tensor.

Table 4
Bond distances (Å) and angles (°) in $[Ru_2(dppe)_2(CO)_6](PF_6)_2$ (**2**)

Metal-ligand distances			
Ru(1)–C(11)	1.907 (4)	Ru(1)–C(13)	1.948 (4)
Ru(1)–C(12)	1.961 (4)	Ru(1)–P(12)	2.3742 (9)
Ru(1)–P(11)	2.4457 (10)	Ru(1)–Ru(1)′	3.0413 (6)
Intraligand distances			
C(11)–O(11)	1.144 (4)	C(12)–O(12)	1.128 (4)
C(13)–O(13)	1.131 (4)	P(11)–C(51)	1.817 (4)
P(11)–C(61)	1.824 (4)	P(11)–C(72)	1.846 (3)
P(12)–C(31)	1.818 (4)	P(12)–C(41)	1.829 (4)
P(12)–C(71)	1.832 (4)		
Ligand-metal-ligand			
C(11)–Ru(1)–C(13)	91.9 (2)	C(11)–Ru(1)–C(12)	87.8 (2)
C(13)–Ru(1)–C(12)	171.90 (14)	C(11)–Ru(1)–P(12)	89.57 (10)
C(13)–Ru(1)–P(12)	88.25 (10)	C(12)–Ru(1)–P(12)	99.84 (10)
C(11)–Ru(1)–P(11)	172.52 (10)	C(13)–Ru(1)–P(11)	87.94 (11)
C(12)–Ru(1)–P(11)	93.38 (10)	P(12)–Ru(1)–P(11)	82.95 (3)
C(11)–Ru(1)–Ru(1)′	86.28 (10)	C(13)–Ru(1)–Ru(1)′	84.68 (9)
C(12)–Ru(1)–Ru(1)′	87.23 (10)	P(12)–Ru(1)–Ru(1)′	171.67 (3)
P(11)–Ru(1)–Ru(1)′	101.15 (2)		
Metal carbonyls			
Ru(1)–C(12)–O(12)	175.9 (3)	Ru(1)–C(11)–O(11)	174.7 (3)
Ru(1)–C(13)–O(13)	175.5 (3)		

3.2. Fluxional behavior of *1*

The line shape of the carbonyl resonance was studied as a function of temperature by $^{13}C\{^{1}H\}$-NMR spectroscopy in order to estimate the energy barrier of the fluxional process exhibited by **1**. At room temperature in solution, the carbonyl environments were averaged to yield a triplet at 211.84 ppm ($J_{CP} = 10.67$ Hz). As the temperature was lowered, the peaks broadened (Fig. 3). The slow-exchange limit was not observed, however, owing to the freezing point of the dimethyl ether solvent (−141.5°C) and instrumental limitations. At temperatures below −133°C further broadening was observed and was attributed, at least in part, to increased viscosity of the solvent close to its freezing point.

Solid-state NMR spectroscopy was used to observe the slow-exchange spectrum of **1**. A sample of ^{13}CO-enriched **1** was prepared as described in Method B, and the CPMAS $^{13}C\{^{1}H\}$-NMR spectrum at room temperature showed three carbonyl environments with peaks at 202, 215, and 221 ppm in a 1:1:1 ratio. The average of these resonances (212.3) was close to the resonance observed in solution. No dynamic behavior was observed in the $^{13}C\{^{1}H\}$-NMR spectrum up to 100°C. Spectral acquisition at higher temperatures was not attempted owing to decomposition of the complex at 120°C. The CPMAS $^{31}P\{^{1}H\}$-NMR spectrum gave two resonances at 77.1 and 59.5 ppm and no broadening was observed at elevated temperature.

3.3. Synthesis of $[Ru_2(dppe)_2(CO)_6][PF_6]_2$ (2)

Complex **2** was prepared from **1** by oxidation using one equivalent of $[Cp_2Fe][PF_6]$ in CH_2Cl_2 at low temperature (Eq. (2)). In the solid state **2** was apparently stable in air for several days, but it decomposed in solution when

$$\mathbf{1} + [Cp_2Fe][PF_6] \xrightarrow[-78°C]{CH_2Cl_2} 1/2[Ru_2(dppe)_2(CO)_6][PF_6]_2 + Cp_2Fe \quad (2)$$

exposed to air and at temperatures above 80°C in CH_2Cl_2, and 1,2-$C_2H_4Cl_2$. Complex **2** was insoluble in hydrocarbon solvents, $CHCl_3$, and CCl_4. The IR spectrum of the carbonyl region of **2** in CH_2Cl_2 was shifted to higher energy relative to **1**, which was consistent with decreased π-back-bonding of the terminal carbonyls to a Ru(I) metal center. The absence of IR stretches in the 1750–1850 cm^{-1} region suggested that all the carbonyls were terminal in solution. The electronic absorption spectrum exhibited an absorption maximum at 386 nm ($\epsilon = 17500\ M^{-1}\ cm^{-1}$), which was assigned to the M–M $\sigma \rightarrow \sigma^*$ transition (Fig. 4) [30] and compares favorably with the previously isolated Ru(I)–Ru(I) dimer $[Ru_2(\mu\text{-bbmb})_2(CO)_6][PF_6]_2$ where $\lambda_{max} = 388$ nm ($\epsilon = 13900\ M^{-1}\ cm^{-1}$) and bbmb is 2,2′-bis[(1,1′-biphenyl-2,2′-diyl)phosphite]-3,3′-di-*t*-butyl-5,5′-dimethoxy-1,1′-biphenyl} [14]. No EPR signal was detected for a 40 mM sample of **2** in CH_2Cl_2 at room temperature.

Table 5
Atomic coordinates ($\times 10^4$) and equivalent isotropic displacement parameters ($Å^2 \times 10^3$) for **2**

Atom	x	y	z	U_{eq}	SOF
Ru(1)	6000 (1)	5625 (1)	985 (1)	23 (1)	1
C(11)	5280 (2)	5864 (2)	1486 (2)	30 (1)	1
O(11)	4859 (2)	5991 (2)	1855 (2)	41 (1)	1
C(12)	5172 (2)	4598 (2)	784 (3)	30 (1)	1
O(12)	4668 (2)	4020 (2)	691 (2)	38 (1)	1
C(13)	6789 (2)	6675 (2)	1004 (2)	31 (1)	1
O(13)	7261 (2)	7277 (2)	1072 (2)	43 (1)	1
P(11)	6960 (1)	5305 (1)	562 (1)	27 (1)	1
P(12)	6347 (1)	5516 (1)	2584 (1)	28 (1)	1
C(31)	5685 (2)	4872 (2)	3467 (2)	30 (1)	1
C(32)	4985 (2)	4286 (2)	3225 (3)	37 (1)	1
C(33)	4515 (3)	3786 (2)	3921 (3)	42 (1)	1
C(34)	4753 (3)	3876 (2)	4866 (3)	42 (1)	1
C(35)	5450 (3)	4456 (2)	5113 (3)	41 (1)	1
C(36)	5919 (2)	4949 (2)	4428 (3)	37 (1)	1
C(41)	6777 (2)	6433 (2)	3176 (2)	33 (1)	1
C(42)	6307 (3)	6711 (2)	3450 (3)	43 (1)	1
C(43)	6602 (3)	7428 (3)	3815 (3)	52 (1)	1
C(44)	7367 (3)	7871 (3)	3904 (3)	61 (1)	1
C(45)	7836 (3)	7606 (3)	3646 (3)	58 (1)	1
C(46)	7540 (2)	6880 (2)	3290 (3)	43 (1)	1
C(51)	7636 (2)	5776 (2)	−400 (3)	31(1)	1
C(52)	8190 (2)	6526 (2)	−292 (3)	45 (1)	1
C(53)	8733 (2)	6885 (3)	−1001 (3)	55 (1)	1
C(54)	8708 (3)	6501 (3)	−1833 (3)	53 (1)	1
C(55)	8162 (2)	5775 (3)	−1959 (3)	45 (1)	1
C(56)	7638 (2)	5410 (2)	−1241 (3)	38 (1)	1
C(61)	6672 (2)	4316 (2)	410 (2)	29 (1)	1
C(62)	7102 (2)	4027 (2)	801 (3)	34 (1)	1
C(63)	6897 (2)	3287 (2)	682 (3)	38 (1)	1
C(64)	6263 (2)	2811 (2)	162 (3)	39 (1)	1
C(65)	5833 (2)	3084 (2)	−237 (3)	41 (1)	1
C(66)	6036 (2)	3832 (2)	−115 (3)	33 (1)	1
C(71)	7073 (2)	5249 (2)	2531 (3)	32 (1)	1
C(72)	7562 (2)	5589 (2)	1646 (2)	32 (1)	1
P(13)	2864 (1)	4023 (1)	2112 (1)	37 (1)	1
F(1)	2328 (4)	3342 (4)	1504 (5)	100 (2)	0.70
F(1B)	2971 (10)	4114 (11)	992 (8)	95 (4)	0.30
F(2)	3403 (4)	4722 (4)	2789 (4)	83 (2)	0.70
F(2B)	2702 (10)	3934 (10)	3191 (9)	69 (3)	0.30
F(3)	3341 (4)	4483 (3)	1228 (4)	88 (2)	0.70
F(3B)	3509 (8)	4801(8)	2289 (12)	100 (4)	0.30
F(4)	3379 (2)	3663(2)	2232 (2)	79 (1)	1
F(5)	2453 (4)	3631(4)	3112 (6)	85 (2)	0.70
F(5B)	2130 (9)	3214 (9)	2017 (15)	105 (4)	0.30
F(6)	2337 (2)	4386(2)	2003 (2)	69 (1)	1

U_{eq} is defined as one third of the trace of the orthogonalized U_{ij} tensor.

3.4. Structure of $[Ru_2(dppe)_2(CO)_6][PF_6]_2$ (2)

Single crystals of **2** were grown from a saturated CH_2Cl_2 solution by careful layering with hexanes at room temperature. Single crystal X-ray diffraction demonstrated that in the solid state complex **2** exists as a Ru(I)–Ru(I) dimer held together with a long metal–metal bond (3.0413(6) Å). The structure is similar to that of $[Ru_2(PPh_3)_2(CO)_4(CH_3CN)_4]^{2+}$, which has a Ru(I)–Ru(I) bond length of 2.8731(8) Å and a similar staggered ligand arrangement [31]. The extreme length of the M–M bond in **2** can be attributed mostly to steric repulsion involving the equatorial phosphines, a smaller contribution may result from Coulombic repulsion between the cationic metal centers. The structure of **2** exhibited a slightly distorted octahedral arrangement of the symmetry-equivalent ruthenium atoms. The bite angle (82.95(3)°) of the dppe ligand was similar to that of **1** (vide supra), and the Ru–CO bond of the carbonyl trans to the equatorial phosphine (1.907(4) Å) is shorter than either of the two M–CO bonds cis to the phosphines (1.961(4) and 1.948(4) Å). The dihedral angle between P(11)–Ru(1)–Ru(1)′–P(11)′ was 148.14(5)°. This large angle reduced the unfavorable steric interactions between the bulky equatorial phosphines. The inward leaning of the trans carbonyls toward M–M bond (C(13)–Ru(1)–(C(12) = 171.90(14)°) was observed in similar M–M bonded dimers (viz. $(Me_3P)(CO)_4OsW(CO)_5$ [32], $Mn_2(CO)_{10}$ and $Re_2(CO)_{10}$) [33].

3.5. NMR spectroscopy of $[Ru_2(dppe)_2(CO)_6][PF_6]_2$ (2)

At ambient temperature **2** exhibited two broad $^{31}P\{^1H\}$ resonances (peak width $W = 100$ Hz) between

40 and 50 ppm and a septet at −141 ppm. The ratio of the integration of each of the $^{31}P\{^1H\}$ peaks, corresponding to two different dppe environments and the PF_6 anions, was 1:1:1 supporting the stoichiometry of a dicationic Ru(I)–Ru(I) dimer of the formulation given in Eq. (2). In the low temperature (−40°C) $^{31}P\{^1H\}$-NMR spectrum the line width narrowed and a pair of triplets were observed (J_{PC} = 5.4 Hz) (Fig. 5a).

At room temperature two sets of carbonyl resonances were observed in the $^{13}C\{^1H\}$-NMR spectrum; a triplet at 200.2 ppm ($J = 10.4$ Hz) and three broad features between 197.9 and 199.5 ppm. At low-temperature (−40°C) the natural-abundance $^{13}C\{^1H\}$-NMR spectrum of **2** in CD_2Cl_2 yielded a doublet of triplets and a doublet of quartets in an integral ratio of 2:1 (Fig. 5b). At lower temperatures these resonances broadened. The NMR spectrum at (−40°C) was consistent with the structure shown in Scheme 1.

The low-temperature $^{31}P\{^1H\}$-NMR spectrum was simulated (Fig. 5a) using $\delta_{Pa} = 43$ ppm ($J_{PaPb} = 7$ Hz; $J_{PaP'} = 4.8$ Hz) and $\delta_{Pb} = 54$ ppm ($J_{PbP} = 7$ Hz; and $J_{PbP} = 4.8$ Hz) and a 4 Hz natural line width. The low-temperature natural-abundance $^{13}C\{^1H\}$-NMR spectrum was also simulated (Fig. 5b) using the parameters $\delta_{Ca} = 199.33$ ppm ($J_{CaP} = 13.4$ Hz; J_{CaP} = 5.5 Hz; $J_{CaPb'} = 3.3$ Hz); $\delta_{Cb} = 197.95$ ppm ($J_{CbPb} = 73$ Hz; $J_{CbPb} = 5.5$ Hz; $J_{CbPb'} = 2.5$ Hz) with 5.3 Hz natural line width. The low-temperature (−60°C) $^{31}P\{^1H\}$-NMR spectrum of ^{13}CO-labeled **2** showed the resonance at 43 ppm partially split by 70 Hz into broad peaks by a trans carbonyl and was consistent with the low temperature $^{13}C\{^1H\}$-NMR spectra.

3.6. Dynamic NMR spectroscopy of *2*

Fig. 6 displays representative experimental and calculated $^{31}P\{^1H\}$-NMR spectra between 10 and 90°C. A simultaneous two-site exchange mechanism (Eq. (3)) was used to model the exchange process. The analysis used four different nuclei with two different configurations; the remaining parameters were obtained from the simulations of the low-temperature $^{31}P\{^1H\}$-NMR spectra (Fig. 5a). A covariant set of rate constants were obtained from the line-shape analysis of the same spectra assuming a four-site exchange mechanism (i.e. non-correlated phosphine exchange) and were related to the first set by a factor of two. The two-site mechanism is favored from other mechanistic criterion (vide infra) and the rates assuming this model were used. The following rates (s^{-1}) were obtained for the temperatures (°C) indicated in parenthesis: 146 (10); 300 (20); 610 (30); 1050 (40); 1900 (50); 3500 (60); 6650 (70); 11700 (80); 20000 (90). The Eyring plot shown in Fig. 7, yielded activation parameters $\Delta H^{\ddagger} = 11.8 \pm 0.15$ kcal mol^{-1} and $\Delta S^{\ddagger} = -6.7 \pm 0.6$ eu. The width of the resonances in the spectra used for the line-shape analysis were > 30 Hz; sufficiently broad to provide well-defined rate constants over the temperature range used for the analysis [34].

The variable-temperature $^{13}C\{^1H\}$-NMR spectra are shown in Fig. 8. The doublet of triplets corresponding to C_a and $C_{a'}$ (−40°C) coalesced near −2°C and formed a triplet at 27°C. The doublet of quartets (−40°C) corresponding to C_b and $C_{b'}$ coalesced at 27°C into a broad feature centered at 198.5 ppm. Further heating to 57°C transformed them into a triplet. A noteworthy feature of these spectra was that the two unique carbonyl environments do not exchange with each other at the fast-exchange limit.

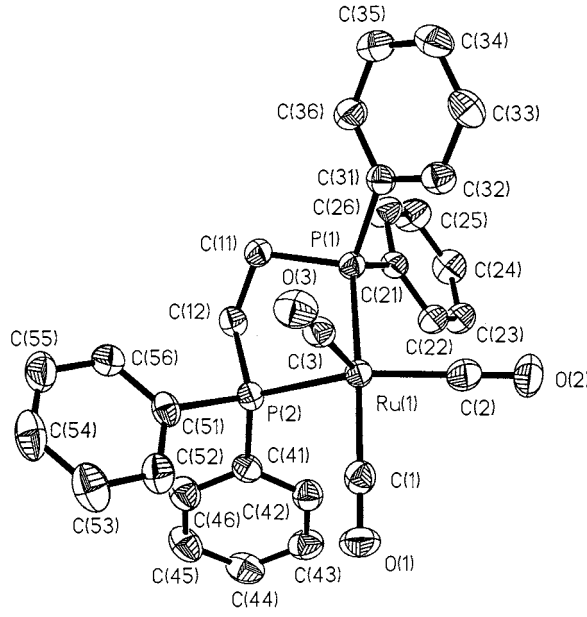

Fig. 1. Structure and labeling scheme for Ru(dppe)$(CO)_3$ **1**. Atoms are depicted as 50% probability ellipsoids, and hydrogen atoms are omitted.

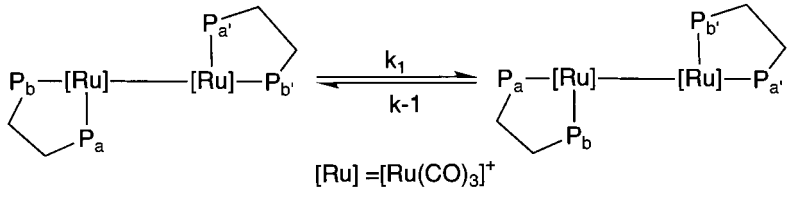

(3)

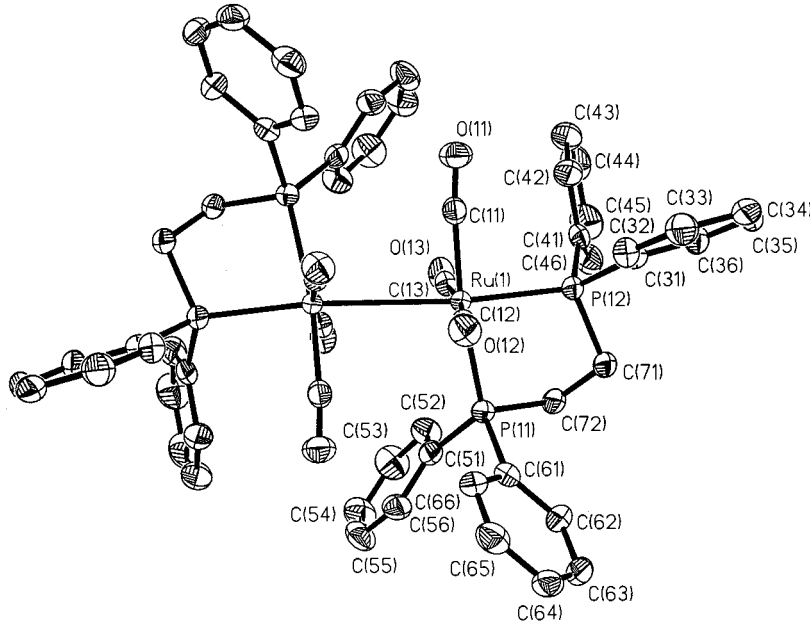

Fig. 2. Structure and labeling scheme for the cation $[Ru_2(dppe)_2(CO)_6]^{2+}$ present in crystalline $[Ru_2(dppe)_2(CO)_6][PF_6]_2$. Atoms are depicted as 50% probability ellipsoids and hydrogen atoms are omitted for clarity. The unlabeled atoms are related to the labeled ones by a two-fold rotation axis.

Line-shape analysis of the C_b and $C_{b'}$ portion of the $^{13}C\{^1H\}$-NMR spectra was performed on the spectra obtained at -2, 27, and 47°C (Fig. 8). The mechanism used to simulate the exchange process is given in Eq (4). This mechanism was modeled by using three different nuclei (P_a, P_b, and C_b) in two different configurations where P_a exchanged with P_b along with parameters based on the simulation of the low temperature spectrum. The following rates (s^{-1}) were obtained for the temperatures (°C) indicated in parenthesis: 50 (-2), 550 (27), 1800 (47) and are plotted along side the rates obtained from the $^{31}P\{^1H\}$-NMR line-shape analysis (Fig. 7).

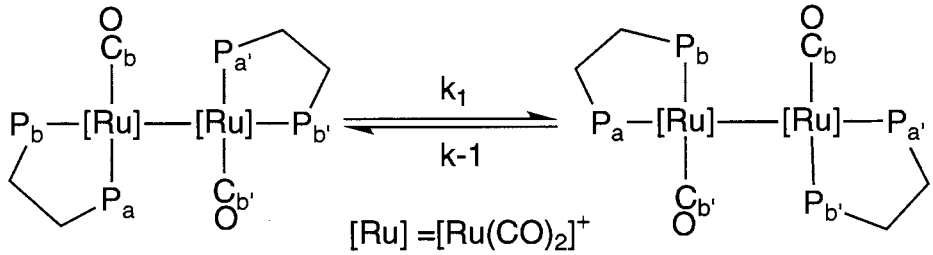

(4)

3.7. Attempted labeling of **2**

A sample of **2** in CH_2Cl_2 was placed under 80 psig of ^{13}CO in a high-pressure sapphire NMR tube. No carbonyl exchange was observed at room temperature during a 48 h period by $^{13}C\{^1H\}$-NMR spectroscopy and the resonance at 185 ppm corresponding to free ^{13}CO in solution remained narrow ($W = 4.5$ Hz) during the course of the experiment. The $^{31}P\{^1H\}$-NMR resonances were not effected by the presence of ^{13}CO.

3.8. Disproportionation of $[Ru_2(dppe)_2(CO)_6][PF_6]_2$ (**2**) in acetonitrile

When **2** was dissolved in acetonitrile and heated to reflux for 30 min a quantitative disproportionation produced **1** and a new compound, $[Ru(dppe)(CO)_2(CH_3CN)_2][PF_6]_2$ (**3**) in a 1:1 ratio as determined by $^{31}P\{^1H\}$-NMR spectroscopy in CD_3CN. The singlets at 74.3 ppm and 64.6 ppm were assigned to **1** and **3** respectively. The reaction was monitored by IR spectroscopy in CH_3CN and yielded four strong stretches; three at 2000, 1926, and 1903 cm^{-1} were assigned to **1** and the fourth (at 2030 cm^{-1}) was assigned to **3**. The same reaction was carried out with a ^{13}CO-enriched sample of **2** in CD_3CN and two triplets were observed in the carbonyl region of the $^{13}C\{^1H\}$-NMR spectrum; one centered at 212.8 ppm ($J_{CP} = 10.3$ Hz) assigned to **1**, and the other centered at 195.6 ppm ($J_{CP} = 15.9$ Hz). The triplets were observed in a 3:2 ratio and the only product consistent with the NMR data was *trans*-$[Ru(dppe)(CO)_2(CH_3CN)_2][PF_6]_2$ (**3**) (Eq. (5)).

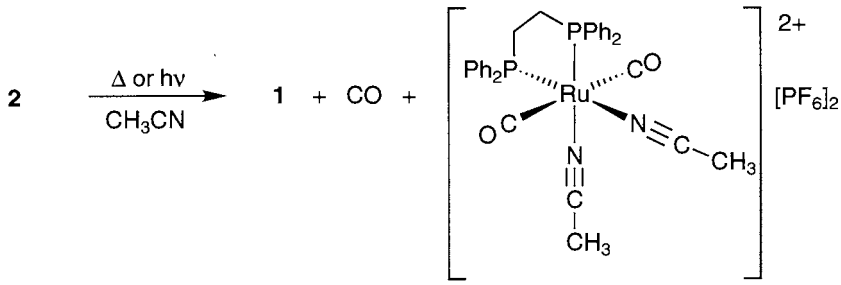

(5)

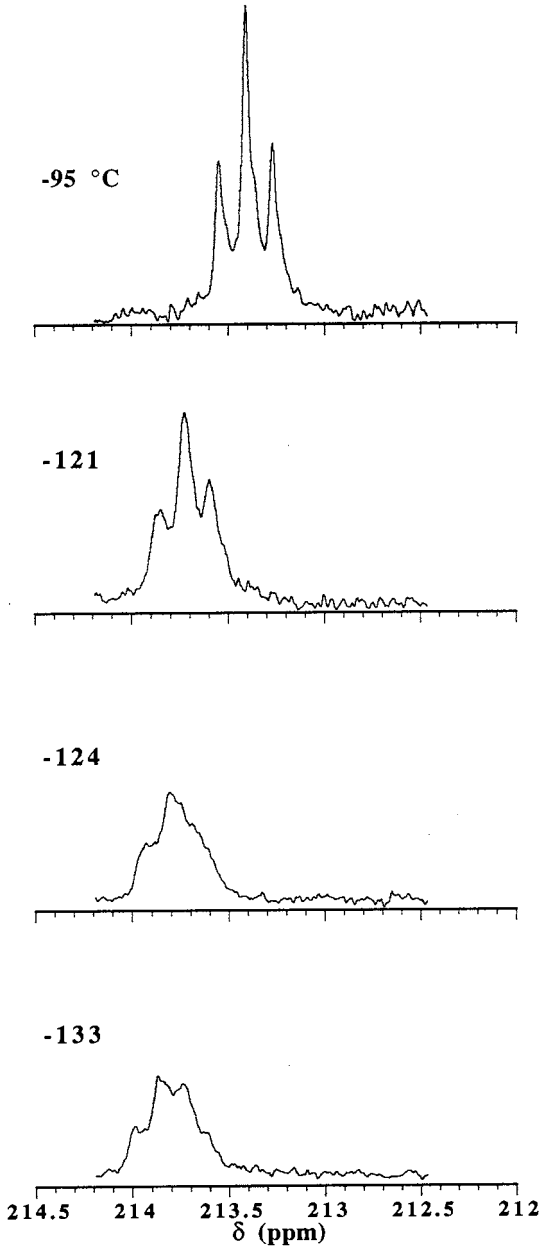

Fig. 3. Variable-temperature (75.4 MHz) $^{13}C\{^1H\}$ NMR spectra in the carbonyl region of a 16 mM solution of a ^{13}CO-labeled sample of $Ru(dppe)(CO)_3$ (**1**) in $(CD_3)_2O$ at the indicated temperatures.

Complex **3** was isolated preparatively as an off-white solid. A methyl resonance was observed at 2.6 ppm in the ^1H-NMR spectrum integrating to six protons relative to the protons of the dppe backbone. The $^{13}C\{^1H\}$-NMR spectrum in CD_2Cl_2 obtained from the same isolated sample yielded a triplet at 195 ppm ($J_{CP} = 15.5$ Hz) and was assigned to the CO resonance of **3**. exhibiting characteristic cis coupling to the phosphorus atoms. These observations were consistent with the structure drawn in Eq. (5).

The same disproportionation reaction was observed to occur photochemically when **2** was placed in a quartz NMR tube and photolyzed for ca. 4 h at 25°C. Three resonances were observed by $^{31}P\{^1H\}$-NMR spectroscopy at 74.3, 64.6, and 72.6 ppm, corresponding to **1**, **3** and a new complex (**4**) in a 2:1:1 ratio respectively. No reaction ($< 5\%$) occurred when an acetonitrile solution of **2** was allowed to sit for a 15 h period in a glass NMR tube exposed to laboratory light.

A photolysis experiment was carried out using a ^{13}CO-enriched sample of **2**, and the same three resonances appeared in the $^{31}P\{^1H\}$-NMR spectrum after ca. 6 h. The phosphorus resonances at 74.3 and 64.8 ppm had characteristic splitting due to isotopic enrichment of ^{13}CO, while the third resonance was a singlet.

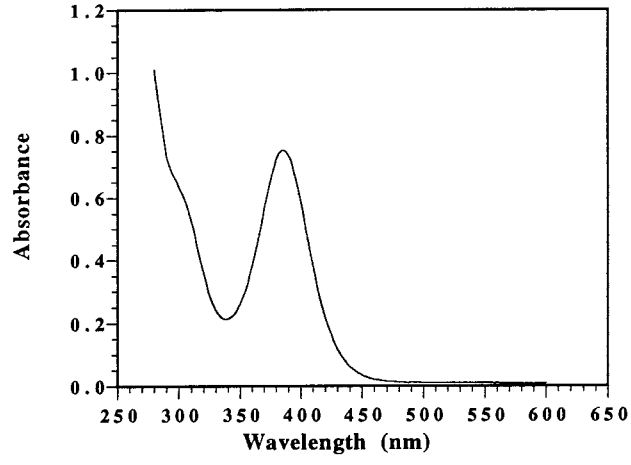

Fig. 4. Electronic absorption spectrum of a 4.53×10^{-5} M solution of $[Ru_2(dppe)_2(CO)_6][PF_6]_2$ (**2**) in CH_2Cl_2 at ambient temperature.

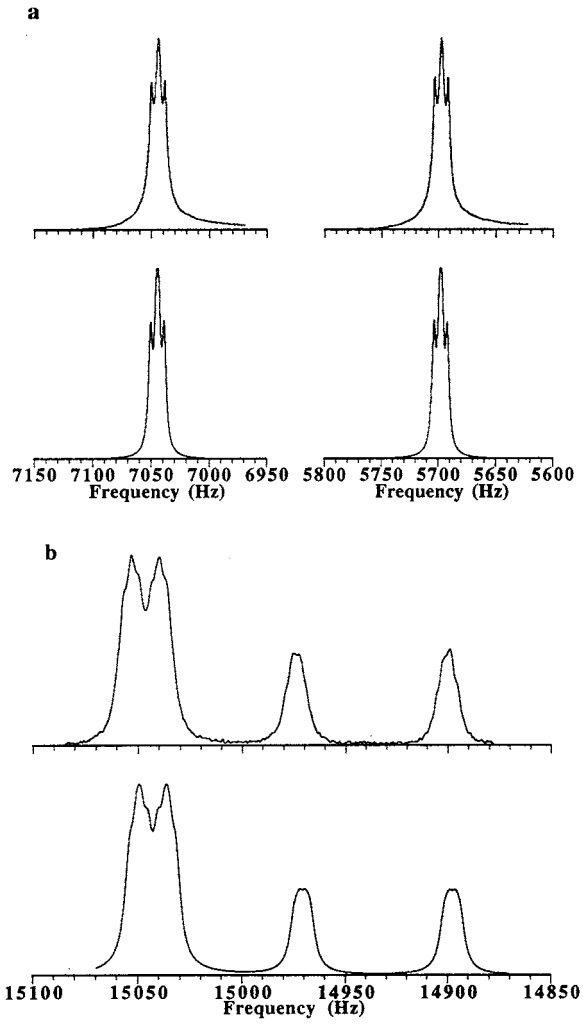

Fig. 5. Actual and simulated natural abundance NMR spectra of a 37 mM solution of $[Ru_2(dppe)_2(CO)_6][PF_6]_2$ (**2**) at -40°C in CD_2Cl_2. The experimental spectra are located above the simulated spectra. (a) (121 MHz) $^{31}P\{^1H\}$ spectrum, (b) (75.4 MHz) natural-abundance $^{13}C\{^1H\}$ spectrum.

After additional photolysis the resonances at 72.6 ppm became larger at the expense of the resonance at 64.6 ppm. Gas evolution was observed in the quartz NMR tube, and the $^{13}C\{^1H\}$-NMR spectrum yielded a triplet at 212.8 ppm ($J_{CP} = 10.4$ Hz) assigned to **1**, a triplet at 195.6 ppm ($J_{CP} = 15.5$ Hz) assigned to **3**, and a singlet located at 185.5 assigned to free gaseous CO.

Complex **3**, which was isolated on a preparative scale, was placed in a quartz NMR tube and photolyzed for 4 h. The reaction was monitored periodically by $^{31}P\{^1H\}$-NMR spectroscopy, and the initial resonance corresponding to **3** at 64.8 ppm was found to be replaced by a resonance at 72.6 ppm. Since no ^{13}CO resonance was detected in **4** by NMR spectroscopy, and because free CO was observed, we assign the $^{31}P\{^1H\}$ singlet at 72.6 ppm to $[Ru(dppe)(CH_3CN)_4]^{2+}$ (Eq. (6)).

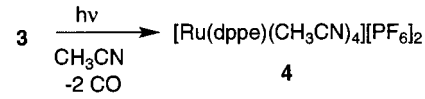

(6)

3.9. Halogen atom abstraction reactions of $[Ru_2(dppe)_2(CO)_6][PF_6]_2$ (2)

When **2** was dissolved in 1,2-$C_2H_4Cl_2$ and heated to ca. 100°C for 30 min, a singlet in the $^{31}P\{^1H\}$-NMR spectrum grew in at 54.6 ppm. When the same reaction was carried out using ^{13}CO-enriched **2** the phosphorus resonance observed at 54.6 ppm was partially split by ^{13}CO into a doublet of doublets ($J_{PCtrans} = 95.2$ Hz, $J_{PCcis} = 15.29$ Hz). Three different sets of resonances were observed in the carbonyl region by $^{13}C\{^1H\}$-NMR spectroscopy: a triplet at 186.04 ppm ($J_{CP} = 11.5$ Hz), a doublet of doublets at 184.64 ppm ($J_{CPtrans} = 94.6$ Hz, $J_{CPcis} = 14.1$ Hz), and characteristic exchanged-broadened resonances at 198–200 ppm corresponding to **2**. The first two sets of resonances were observed in a 1:2 ratio. From the these NMR experiments, this new species was assigned as *fac*-$[Ru(dppe)(CO)_3Cl][PF_6]$ (**5**) (Eq. (7)).

This structural assignment

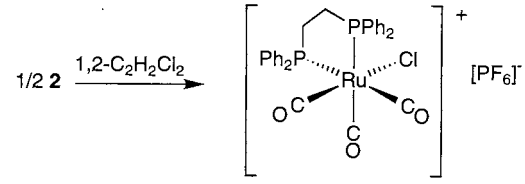

5

(7)

was also consistent with the IR spectrum (ν_{CO}; 2135 (s), 2097 (s), and 2053 (s) cm^{-1}). From a sample isolated via photolysis (vide infra) four sets of triplets were observed in the aryl region of the $^{13}C\{^1H\}$ spectrum and was consistent with the NMR spectral patterns observed in the isostructural species *fac*-Re(dppe)$(CO)_3$(OMe) [29].

Complex **5** was unstable at elevated temperatures. When heated to ca. 100°C for 1 h, two new unknown species grew in at the expense of **5** by as monitored by $^{31}P\{^1H\}$-NMR spectroscopy. These species exhibited a singlet at 69.8 ppm, and a pair of doublets at 68.9 ppm and 68.3 ppm ($J_{PC} = 14.6$ Hz) in a 3:7 ratio. The same experiment was carried out using ^{13}CO-enriched **2** and three sets of resonances were observed in the carbonyl region of the $^{13}C\{^1H\}$ spectrum: a multiplet at 199.8 ppm, a triplet at 196.0 ($J_{CP} = 16.1$ Hz), and a singlet at 184.5 ppm (assigned as free CO). No further attempts were made to identify these two compounds.

A similar halogen atom abstraction reaction was observed between **2** and 1,2-$C_2H_4Cl_2$ carried out at 25°C under photochemical conditions. Complex **5** would slowly grow in upon photolysis of **2** in a quartz NMR tube. After 4 h of photolysis **2** was completely

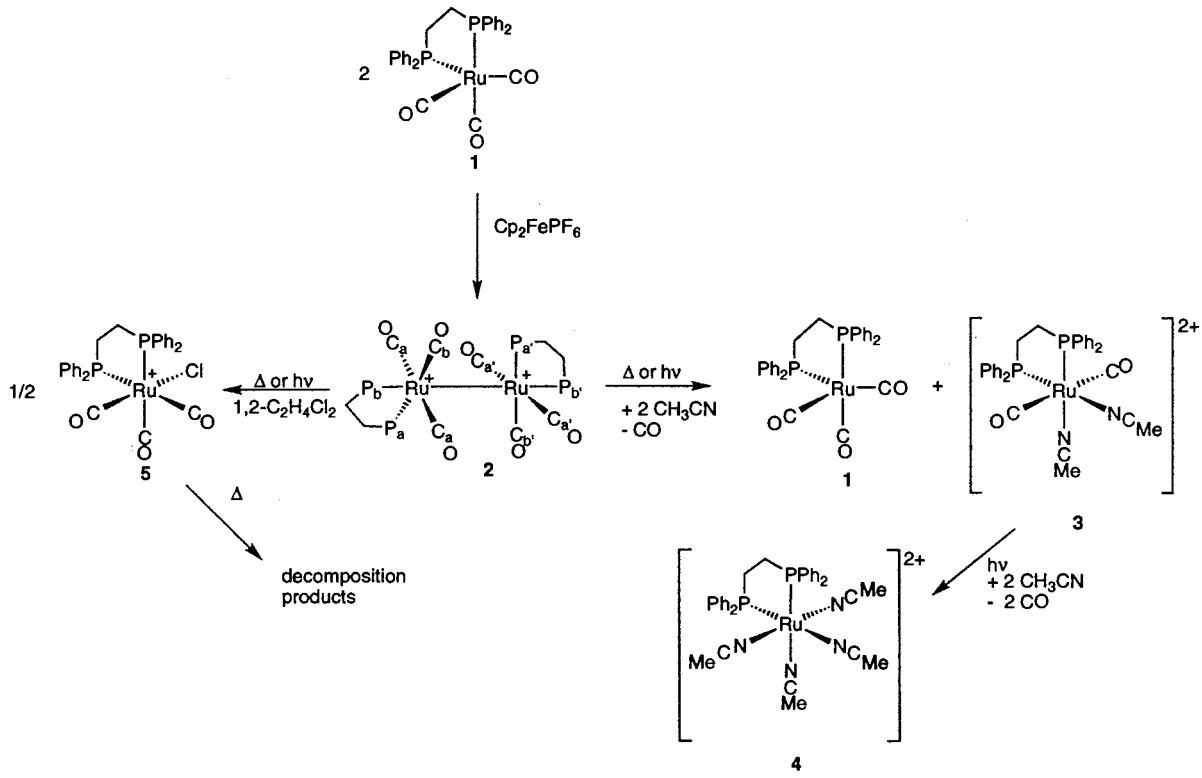

Scheme 1.

converted to **5** in addition to a small amount of another unidentified species as evidenced by the appearance of singlets at 54.58 ppm and 57.94 ppm (7:3 ratio) in the $^{31}P\{^{1}H\}$-NMR spectrum.

In contrast to **3**, complex **5** was photochemically stable, but thermally unstable. A sample of **5** generated under thermal conditions was transferred to a quartz NMR tube and photolyzed for 2 h. There was no change in the $^{31}P\{^{1}H\}$ spectrum during the course of the experiment. This same sample was then heated to 100°C for 45 min, and **5** was converted to the two unidentified species described above. These findings provided a method to isolate **5** at room temperature on a preparative scale via photolysis.

4. Discussion

4.1. Fluxional behavior of $Ru(dppe)(CO)_3$

From previous work we discovered that a rate determining electron-transfer step occurred in the reaction between **1** and nitroarenes (Eq. (1)). A large intrinsic barrier was measured ($\Delta G^{\ddagger}(0) = 14$ kcal mol^{-1} at 25°C) for the electron-transfer reaction [35]. Part of this reorganization energy was thought to involve a conformational change of **1** from trigonal bipyramidal (tbp) to square pyramidal (spy), which would be required to form the octahedral product. This conformational change was related to the fluxional process which interconverts the two inequivalent phosphorus atoms of the dppe ligand. Based on previous studies of the fluxional behavior of five coordinate complexes (viz. $Fe(CO)_5$, $Ru(CO)_5$ and $Fe(dppe)(CO)_3$) [36] we felt that the barrier might be measurable by a combination of low temperature and solid state NMR techniques.

The combination of the data collected from the solution and solid state NMR studies allowed an estimation of the energy barrier of the fluxional process for **1**. The solid state NMR studies provided the chemical shift difference between the axial and equatorial carbonyls ($\delta\nu$ ca. 1200 Hz) in complex **1** at the slow-exchange limit. From the solution state $^{13}C\{^{1}H\}$-NMR studies the coalescence temperature was estimated to be -135 ± 10°C. Using an expression relating the rate constant to the peak separation of the two sites at the coalescence temperature ($k = \pi\delta\nu 2^{-1/2}$), we estimated the rate constant to be 2660 s^{-1} [17]. From this value we estimate $\Delta G^{\ddagger}_{138}$ for the exchange process to be 6 kcal mol^{-1}.

4.2. Fluxional behavior of $[Ru_2(dppe)_2(CO)_6][PF_6]_2$

Several different mechanisms for the fluxional behavior of **2** can be postulated: phosphine or carbonyl

dissociation, trigonal twist, Ru(I)–Ru(I) bond homolysis, and exchange through bridging carbonyls. At the fast-exchange limit the $^{13}C\{^1H\}$-NMR spectrum shows that C_a and C_b do not exchange with one another. Each of the resonances retain coupling to the ^{31}P nuclei under conditions of both slow and fast exchange (Fig. 8) indicating that the exchange process is intramolecular [37]. The quantitative agreement between the line-shape analysis of the $^{31}P\{^1H\}$- and $^{13}C\{^1H\}$- dynamic NMR (DNMR) spectra implies that the rate of exchange of the phosphorus atoms was the same as that of the carbon atoms. The observation that no exchange was observed between **2** and gaseous ^{13}CO rules out a mechanism involving ligand dissociation. A trigonal-twist mechanism, often invoked for carbonyl exchange in $M(CO)_3$ units of clusters [38], can be eliminated because it would require exchange between C_a and C_b. Exchange involving Ru(I)–Ru(I) bond homolysis would involve generation of a five-coordinate metal-centered radical intermediate that could undergo rapid exchange followed by radical recombination. This mechanism can also be ruled out because it would involve scrambling of C_a and C_b.

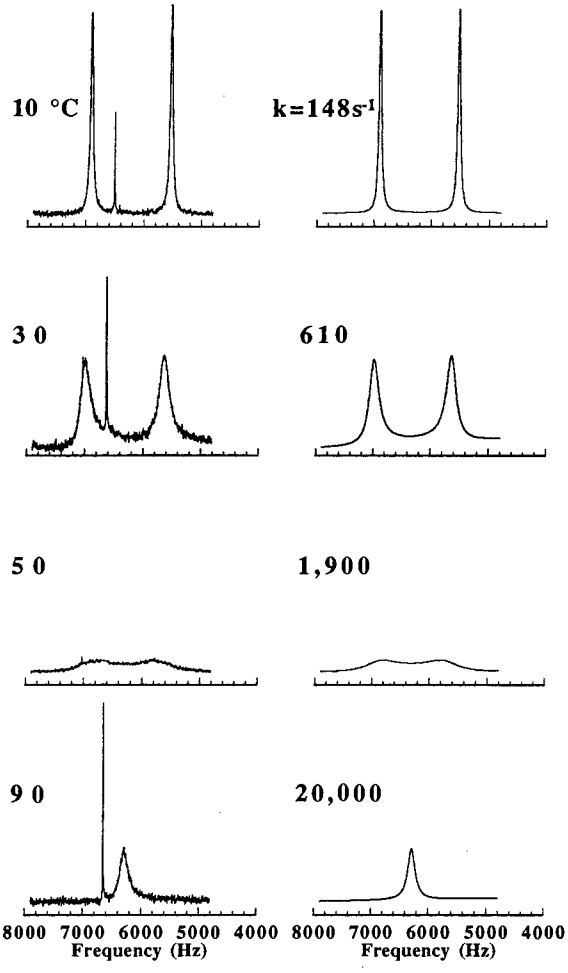

Fig. 6. Representative spectra of the experimental and simulated (121 MHz) $^{31}P\{^1H\}$ NMR spectra of a 37 mM solution of $[Ru_2(dppe)_2(CO)_6][PF_6]_2$ (**2**) at the indicated temperatures. The experimental spectra are in the left column, and the simulated spectra are in the right column with corresponding rate constants used for the simulation. At elevated temperatures **2** would decompose in CD_2Cl_2 and 1,2-$C_2H_2Cl_2$ to form *fac*-$[Ru(dppe)(CO)_3Cl][PF_6]$ (see results), which exhibits a resonance at 54.6 ppm and can be seen in the various spectra and was omitted in the spectrum at 50°C for clarity.

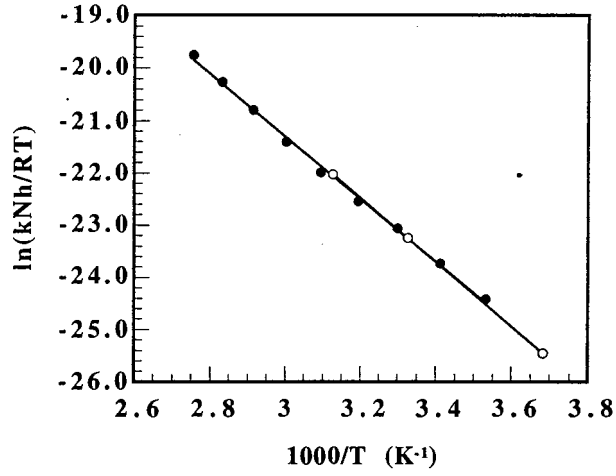

Fig. 7. Eyring plot of the rates of exchange using the model described in the text at different temperatures: (●) rates obtained from $^{31}P\{^1H\}$ NMR line-shape analysis, (○) rates obtained from $^{13}C\{^1H\}$ NMR line-shape analysis.

The bridging carbonyl mechanism is depicted in Scheme 2 [39]. It involves migration of the carbonyls trans to the phosphines to form a bridged intermediate, which affords the exchanged product upon opening of the bridges. This mechanism does not involve exchange between the different carbonyl environments and was consistent with the agreement between the rates obtained from the line-shape analysis of the $^{13}C\{^1H\}$ and $^{31}P(^1H\}$ DNMR spectra (Fig. 7). Although other stereochemistries of the bridged intermediate could be drawn these exchange pathways lead to exchange between C_a and C_b.

Exchange of terminal carbonyls through bridged intermediates is well-known in examples including $Os_3(CO)_{12-x}L_x$ clusters (where L can be various combinations of CO or PR_3) [40–42] as well as in $(Me_3P)(CO)_4OsW(CO)_5$ [32], and $MnRe(CO)_{10}$ [43]. Alex and Pomeroy have measured the activation energy for this process for $Os_3(CO)_{11}[P(OMe)_3]$ where $\Delta G^{\ddagger}_{293} = 14$ kcal mol^{-1} and compares favorably to the activation energy measured for the exchange process of **2** where $\Delta G^{\ddagger}_{293} = 13.8$ kcal mol^{-1}. Schmidt et al. measured the activation parameters for the exchange of ^{13}CO between the two metal centers of $Re(^{13}CO)_5Mn(CO)_5$ and found $\Delta H^{\ddagger} = 12.7 \pm 1.4$ kcal mol^{-1} and $\Delta S^{\ddagger} = -41 \pm 6$ eu [43]. This value for the

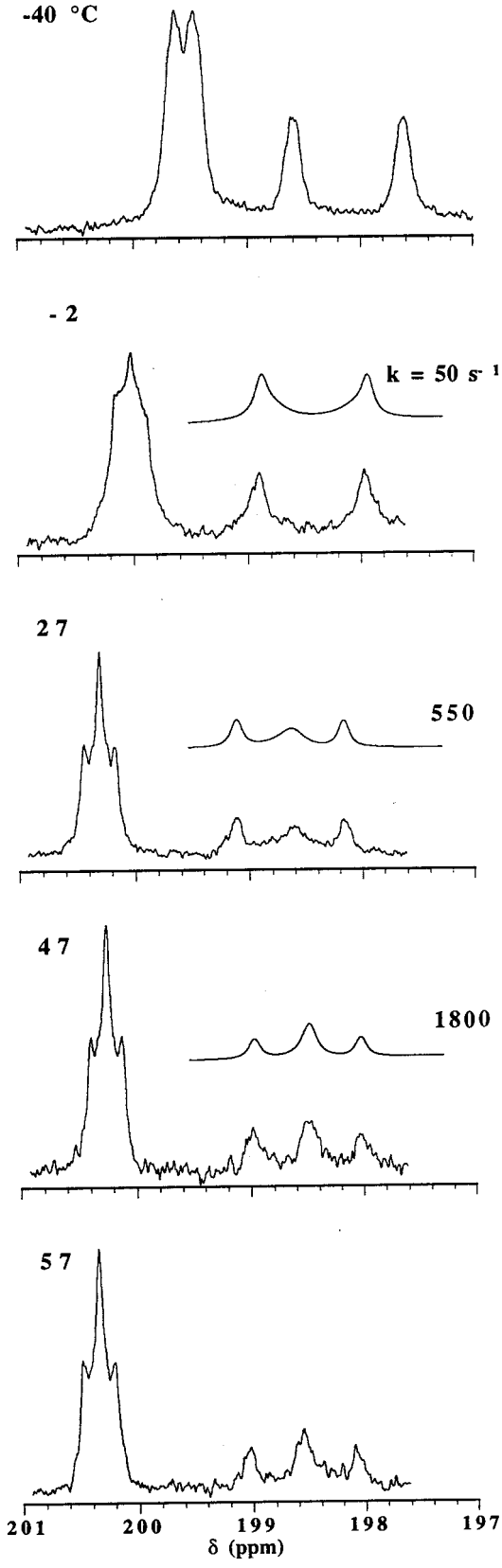

Fig. 8. Variable-temperature (75.4 MHz) $^{13}C\{^{1}H\}$ NMR spectra in the carbonyl region of a 37 mM solution ^{13}CO-labeled $[Ru_2(dppe)_2(CO)_6][PF_6]_2$ (**2**) at the indicated temperatures. The simulated spectra are shown above the experimental spectra with corresponding rate constants.

enthalpy of reaction compared favorably to $\Delta H^{\ddagger}$ for the exchange process for **2** (11.8 kcal mol^{-1}) but the $\Delta S^{\ddagger}$ for **2** (-6.7 eu) was much larger than that for $Re(^{13}CO)_5Mn(CO)_5$.

4.3. Thermal and photochemical disproportionation of $[Ru_2(dppe)_2(CO)_6][PF_6]_2$

Although other mechanistic possibilities exist, based on ample precedent [10,11,44–47] the disproportionation of **2** in CH_3CN is thought to involve initial metal–metal bond rupture to form a $17e^-$ species (Eq. (8)), followed by substitution of a carbonyl (Eq. (9)). A second CH_3CN addition forms a $19e^-$ species (Eq. (10)) prompting an electron transfer to another radical cation (Eq. (11)) to yield products **1** and **3**.

$$[Ru_2(dppe)_2(CO)_6]^{2+} \xrightarrow{h\nu \text{ or } \Delta} 2[Ru(dppe)(CO)_3]^{\bullet +} \quad (8)$$

$$[Ru(dppe)(CO)_3]^{\bullet +} + MeCN \rightarrow [Ru(dppe)(CO)_2MeCN]^{\bullet +} + CO \quad (9)$$

$$[Ru(dppe)(CO)_2MeCN]^{\bullet +} MeCN \rightarrow [Ru(dppe)(CO)_2(MeCN)2]^{\bullet +} \quad (10)$$

$$[Ru(dppe)(CO)_2(MeCN)_2]^{\bullet +} + [Ru(dppe)(CO)_3]^{\bullet +} \rightarrow [Ru(dppe)(CO)_2(MeCN)_2]^{2+} + Ru(dppe)(CO)_3 \quad (11)$$

The bond dissociation energy for dimers containing M–M bonds was reported to be 28 kcal mol^{-1} for $Mn_2(CO)_8(PPh_3)_2$ [48], 25 kcal mol^{-1} for $Fe(\eta^5\text{-}C_5H_5)(CO)_2]_2$, and 22 kcal mol^{-1} for $[Mo(\eta^5\text{-}C_5H_5)(CO)_3]_2$ [49]. Substitution of a phosphine for a CO ligand weakens M–M bonds for both steric and electronic reasons [50]. For example $Mn_2(CO)_{10}$ fails to undergo thermal M–M bond homolysis [51,52], but $Mn_2(CO)_8(PPh_3)_2$ [48] and $Mn_2(CO)_6(depe)_2$ (where depe is 1,2 bis(diethylphosphino)ethane) [53] undergo spontaneous M–M bond homolysis upon heating. Similar findings were observed by Brown and coworkers by synthesizing persistent metal centered radicals with bulky phosphine ligands $Mn(CO)_3(P(i\text{-}Bu)_3)_2$ [54]. Within a group the strength of M–M bonds increases upon descending the triad [55]. The effects of substitution and metal size are compensating in the case of **2**. In addition to the above mentioned effects, the dicationic nature of **2** may further weaken the Ru(I)–Ru(I) bond due to electrostatic effects.

If we assume that the thermal reactions exhibited by **2** occur by rate determining bond cleavage, we would be able to provide a rough measure of the energetics of M–M bond rupture. This assumption is consistent with the observed correlation between products of the thermal and photochemical reactions [56]. A first-order rate of 1.8×10^{-5} s^{-1} was mea-

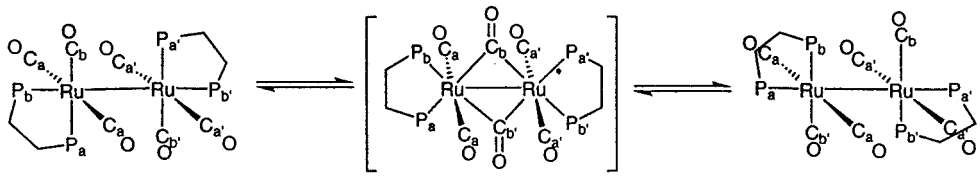

Scheme 2.

sured (at 50°C by IR spectroscopy of a 3.4 mM solution of **2**) for the disproportionation reaction corresponding to $\Delta G^{\ddagger}_{323} = 26$ kcal mol^{-1}. This represents a reasonable value for the M–M bond homolysis process [50].

4.4. Halogen atom abstraction

Irradiation of $M_2(CO)_8L_2$ (where L is a monodentate or bidentate phosphine and M = Mn, Re) causes M–M bond homolysis and in the presence of alkyl halides halogen atom abstraction occurs [57]. The predominant isomer formed from halogen atom abstraction reactions in the Mn systems containing bidentate phosphines is *fac*-$Mn(CO)_3L_2X$ [53].

Of the two possible isomers for the halogen atom abstraction of **2** only the *fac*-$[Ru(dppe)(CO)_3Cl]^+$ isomer was formed. One possible reaction sequence invoking intermediates **A** and **B** to rationalize the observed products is depicted in Scheme 3. The equilibrium between intermediates **A** and **B** would be necessary to form the observed products. Similar equilibria have been proposed to account for the observed preference for phosphine ligands to occupy the basal position of sqpy Mn complexes generated upon photolysis of the corresponding dimers [54,58].

The rate of the halogen atom abstraction reaction at 70°C was estimated (from the half-life assuming a first-order dependence on **2** by $^{31}P\{^1H\}$-NMR spectroscopy) to be ca. 4×10^{-4} s^{-1} corresponding to $\Delta G^{\ddagger}_{343}$ ca. 26 kcal mol^{-1}. This activation barrier was similar to that of the disproportionation reaction and consistent with the proposed M–M bond homolysis mechanism.

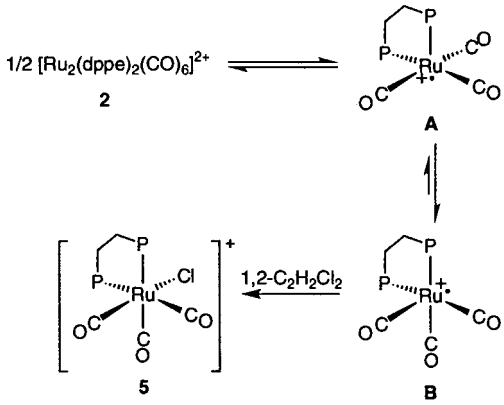

Scheme 3.

Acknowledgements

We thank Ken Caulton for helpful conversations. The research was supported by a grant from the National Science Foundation (CHE-9223433)

References

[1] S.J. Skoog, J.P. Campbell, W.L. Gladfelter, Organometallics 13 (1994) 4137.
[2] S.J. Sherlock, D.C. Boyd, B. Moasser, W.L. Gladfelter, Inorg. Chem. 30 (1991) 3626.
[3] J.D. Gargulak, A.J. Berry, M.D. Noirot, W.L. Gladfelter, J. Am. Chem. Soc. 114 (1992) 8933.
[4] A.J. Kunin, M.D. Noirot, W.L. Gladfelter, J. Am. Chem. Soc. 111 (1989) 2739.
[5] J.K. Kochi, Organometallic Mechanism and Catalysis, Academic Press, New York, 1978.
[6] S.W. Blanch, A.M. Bond, R. Colton, Inorg. Chem. 20 (1981) 755.
[7] P.K. Baker, N.G. Connelly, B.M.R. Jones, J.P. Maher, K.R. Somers, J. Chem. Soc. Dalton Trans. (1980) 579.
[8] P.K. Baker, K. Broadley, N.G. Connelly, J. Chem. Soc. Dalton Trans. (1982) 471.
[9] W.C. Trogler, in: W.C. Trogler (Ed.), Organometallic Radical Processes, Elsevier, Amsterdam 1990, pp. 306–337.
[10] M.J. Therien, C.-L. Ni, F.C. Anson, J.G. Osteryoung, W.C. Trogler, J. Am. Chem. Soc. 108 (1986) 4037.
[11] L. Song, W.C. Trogler, J. Am. Chem. Soc. 114 (1992) 3355.
[12] N.G. Connelly, W.E. Geiger, Adv. Organomet. Chem. 23 (1984) 1.
[13] N.G. Connelly, Chem. Soc. Rev. 18 (1989) 153.
[14] B. Moasser, C. Gross, W.L. Gladfelter, J. Organomet. Chem. 471 (1994) 201.
[15] B.J. Burger, J.E. Bercaw, in: A.L. Wayda, M.Y. Darensbourg (Eds.), Experimental Organometallic Chemistry, vol. 357, American Chemical Society, Washington D.C. 1987, pp. 79–98.
[16] D.N. Hendrickson, Y.S. Sohn, H.B. Gray, Inorg. Chem. 10 (1971) 1559.
[17] J. Sandstrsm, Dynamic NMR Spectroscopy, Academic Press, London, 1982.
[18] D.C. Roe, J. Mag. Res. 63 (1985) 388.
[19] R.A. Sanchez-Delgado, J.S. Bradley, G. Wilkinson, J. Chem. Soc. Dalton Trans. (1976) 399.

[20] A.J. Gordon, R.A. Ford, The Chemist's Companion, John Wiley and Sons, New York, 1972.
[21] G. HSegele, S. Goudestsidis, H.W. Hsffken, T. Lenzen, R. Spiske, U. Weber, Phosphorus Sulphur Silicon 77 (1993) 262.
[22] A. Pines, M.G. Gibby, J.S. Waugh, J. Chem. Phys. 59 (1973) 569.
[23] SHELXTL-plus V5.0, Siemens Industrial Automation, Inc., Madison, WI, 1995.
[24] G.M. Sheldrick, Acta Crystallogr. A46 (1990) 467.
[25] A.L. Spek, Acta. Cryst. A46 (1990) C34.
[26] A.J.C. Wilson, International Tables for Crystallography, Vol. C, Kluwer Academic Publishers, Dordrecht, 1995.
[27] J.D. Gargulak, W.L. Gladfelter, Inorg. Chem. 33 (1994) 253.
[28] L.P. Battaglia, D. Delledonne, M. Nardelli, C. Pelizzi, G. Predieri, G.P. Chiusoli, J. Organomet. Chem. 330 (1987) 101.
[29] S.K. Mandal, D.M. Ho, M. Orchin, Inorg. Chem. 30 (1991) 2244.
[30] R.A. Levenson, H.B. Gray, J. Am. Chem. Soc. 97 (1975) 6042.
[31] W.G. Klemperer, B. Zhong, Inorg. Chem. 32 (1993) 5821.
[32] F.W.B. Einstein, T. Jones, R.K. Pomeroy, P. Rushman, J. Am. Chem. Soc. 106 (1984) 2707.
[33] M.R. Churchill, K.N. Amoh, H.J. Wasserman, Inorg. Chem. 20 (1981) 1609.
[34] G. Binsch, H. Kessler, Angew. Chem. Int. Ed. Engl. 19 (1980) 411.
[35] S.J. Skoog, W.L. Gladfelter, J. Am. Chem. Soc. 119 (1997) 11049.
[36] M. Akhtar, P.D. Ellis, A.G. MacDiarmid, J.D. Odom, Inorg. Chem. 11 (1972) 2917.
[37] M.A. Gallop, B.F.G. Johnson, J. Lewis, J. Chem. Soc. Chem. Commun. (1987) 1831.
[38] R.F. Alex, R.K. Pomeroy, Organometallics 6 (1987) 2437.
[39] E. Band, E.L. Muetterties, Chem. Rev. 78 (1978) 639.
[40] A. Forster, B.F.G. Johnson, J. Lewis, T.W. Matheson, B.H. Robinson, W.G. Jackson, J. Chem. Soc. Chem. Com. (1974) 1042.
[41] A.J. Demming, S. Donovan-Mtunzi, S.E. Kabir, J. Organomet. Chem. 281 (1985) C43.
[42] R.F. Alex, R.K. Pomroy, Organometallics 6 (1987) 2437.
[43] S.P. Schmidt, F. Basolo, C.M. Jensen, W.C. Trogler, J. Am. Chem. Soc. 108 (1986) 1894.
[44] M. Absi-Halabi, J.D. Atwood, N.P. Forbus, T.L. Brown, J. Am. Chem. Soc. 102 (1980) 6248.
[45] A. Sisak, L. Mark-, J. Organomet. Chem. 330 (1987) 201.
[46] A.E. Stiegman, D.R. Tyler, Acc. Chem. Res. 17 (1984) 61.
[47] S.B. McCullen, T.L. Brown, Inorg. Chem. 20 (1981) 3528.
[48] A. Poë, C.V. Sekhar, J. Am. Chem. Soc. 107 (1985) 4874.
[49] J.R. Pugh, T.J. Meyer, J. Am. Chem. Soc. 114 (1992) 3784.
[50] R.A. Jackson, A. Poë, Inorg. Chem. 17 (1978) 997.
[51] D. Sonnenberger, J.D. Atwood, J. Am. Chem. Soc. 102 (1980) 3484.
[52] S.P. Schmidt, W.C. Trogler, F. Basolo, Inorg. Chem. 21 (1981) 1698.
[53] D.R. Tyler, A.S. Goldman, J. Organomet. Chem. 311 (1986) 349.
[54] S.B. McCullen, T.L. Brown, J. Am. Chem. Soc. 104 (1982) 7496.
[55] J.A. Connor, H.A. Skinner, in: M.H. Chisholm (Ed.), Reactivity of Metal–Metal Bonds, Vol. ACS Symp. Ser. No 155, American Chemical Society, Washington D.C., 1981, pp. 197–205.
[56] D.R. Tyler, Prog. Inorg. Chem. 36 (1988) 125.
[57] M.C. Baird, Chem. Rev. 88 (1988) 1217.
[58] H.W. Walker, G.B. Rattinger, R.L. Belford, T.L. Brown, Organometallics 2 (1983) 775.